



国际竞赛 科研科创 发表论文  
关注“有方背景提升”

# Patterns and Symmetries in Spiking Neural Networks

## **Author**

Victoria Zhang

Phillips Academy

Andover, MA 01810, USA

## **Instructor**

Dr. Bolun Chen

Brandeis University

Waltham, MA 02453, USA



---

# PATTERNS AND SYMMETRIES IN SPIKING NEURAL NETWORKS

---

Victoria Zhang

## ABSTRACT

The human brain, which consists of about 100 billion nerve cells, is arguably the most complex system in nature. Deciphering its working mechanism poses one of the greatest challenges to physicists, neuroscientists, and mathematicians. Inspired by recent progress in computational neuroscience and artificial intelligence, this paper explores rich temporal patterns in networks of neurons that communicate via electric pulses known as spikes. In particular, we describe the attractors in small circuits of spiking neurons with different connectivity and symmetries. Using methods developed in the theory of dynamical systems, we extend an analytical approach to capture the phase-locked states and their stability for a general  $N$ -cell system. We then systematically explore attractors in reduced state spaces via Poincaré maps for both all-to-all coupled and star-like coupled networks. We identify a sequence of bifurcations when the coupling strengths vary from inhibition to excitation. Moreover, using high-precision numerical simulations, we find two novel states unobserved in the all-to-all network: the death of oscillation for inhibitory coupling and quasi-periodic behaviors for excitatory coupling as possible patterns in a star network. Large networks can be characterized by local components (motifs) as star networks with various degrees. Thus our results elucidate the interplay between dynamical patterns and symmetries in the building block of real networks. Furthermore, since self-sustained oscillations with pulsatile couplings are ubiquitous, our analysis may clarify understanding of not only neural dynamics but also of other pulse-coupled oscillator systems such as non-linear electric circuits, wireless sensor networks, and self-organizing chemical reactions.

**Keywords** Nonlinear Dynamics, Poincaré Map, Bifurcation, Leaky Integrate-and-Fire Neuron, All-to-All, Star-like Network, Death of Oscillation, Limit Cycle, Cluster Synchrony, Synchrony, Attractor



## Table of Contents

<b>1</b>	<b>Introduction</b>	<b>3</b>
<b>2</b>	<b>Integrate and Fire Model</b>	<b>4</b>
<b>3</b>	<b>Dimensional Reduction</b>	<b>5</b>
<b>4</b>	<b>An Analysis of Phase-Locked Solutions</b>	<b>5</b>
4.1	A Review of Two-Cell Systems . . . . .	7
4.2	Three-Cell Systems . . . . .	9
4.3	Higher Order Systems . . . . .	10
<b>5</b>	<b>Dynamics of Small Networks with Different Symmetries and Connectivity</b>	<b>11</b>
5.1	All-to-All Coupling . . . . .	11
5.1.1	Three-Cell System . . . . .	11
5.1.2	Four-Cell System . . . . .	12
5.2	Star Network Coupling . . . . .	13
5.2.1	General Discussion . . . . .	13
5.2.2	Uniform Star Network Coupled Systems . . . . .	14
<b>6</b>	<b>Discussion</b>	<b>16</b>
<b>7</b>	<b>Acknowledgements</b>	<b>19</b>



## 1 Introduction

Due to a balance between energy supply and dissipation, many nonlinear systems in nature exhibit self-sustained oscillations, such as flashing fireflies [1], bursting pacemaker cells [2], chirping crickets [3], and chorusing tree frogs [4]. In particular, nerve cells or neurons in the human brain can elicit periodic pulses in their membrane potential. These periodic pulses are known as spikes, with which neurons communicate and transmit information. Spiking neurons, or more precisely, their dynamical patterns, are the basic element of motor-control [5, 6], perception [7], memory consolidation and retrieval [8], and other high-level cognitive functions [9]. Spiking neurons are the basic element of perception, cognition, and other high-level brain functions. Many works [10, 11, 12] have demonstrated the computing capability of a network of such spiking neurons. Others have suggested neural-inspired algorithms [13, 14, 15] to improve the performance of artificial neural networks (ANN). Recent years have seen a resurgence in the study of ANN and its broad applications to scientific research and the industry [16]. A deep understanding of neural dynamics is therefore undoubtedly of a broad interest in physics, neuroscience, and artificial intelligence.

From a mathematical perspective, a single neuron is a multi-dimensional nonlinear dynamical system [17]. Periodic spikes in the membrane potential correspond to stable limit cycles in the state space. One may use a phase-like variable to describe the neuron's state on the limit cycle [18]. Small perturbations only slightly deform the limit cycle and shift the phase. Thus, unlike a simple harmonic oscillator, the rigidity of the limit cycle renders a neuron adaptive to driving stimuli by adjusting its phase. Entrainment can occur when the cell receives external currents or inputs from other cells. Because a neuron in a network often makes contact with multiple neurons via synapses, rich dynamics emerge as a result of mutual entrainment [19].

It is well known that a network's dynamics can be largely affected by its connectivity, which is described by the adjacency matrix of the underlying graph [20, 21]. If the adjacency matrix is invariant under permutation of nodes, then the network is said to have a certain symmetry, under which the equations of motion of involved nodes stay unchanged. It implies that the invariant nodes are indistinguishable if they form a cluster. Indeed, earlier works [22, 23, 24, 25] established a beautiful link between the symmetry of a network and the clustered states (synchronous patterns) that can exist. But existence does not necessarily guarantee stability. It is the dynamical equations that determine which states are stable [26] and that can be easily observed in numerical simulations or experiments.

And as for spiking neurons, the inter-neuronal synaptic coupling plays a decisive role. Depending on the type of the synapse (excitatory or inhibitory) as well as its activation speed, a network of spiking neurons can exhibit a multitude of patterns, such as full synchrony [27, 28], clustered synchrony and quasi-periodic oscillations [29], and an asynchronous splay state [30]. In these works, the authors assumed an all-to-all coupled neural network (shown in Fig. 1) which has the most symmetry. A natural question therefore arises: what patterns can a network exhibit if the graph has less symmetry?

In this paper, we address this question by considering identical spiking neurons coupled in a star-like network as shown in Fig. 2. In this simple but non-trivial case, a central hub interacts simultaneously with multiple subordinate cells. As information is transferred among local units, this structure acts as a building block (a motif) of large networks, and can be found in many real-world systems such as superconducting junction arrays [31], computer networks [32], and mammalian brains [33].

Specifically, we model a neuron as a leaky integrate-and-fire (LIF) oscillator, a widely-used model in neuroscience and applied mathematics. We extend an analytical approach developed in Ref. [34] to capture the phase-locked states and their stability for  $N$  coupled neurons as an analytic function. Using high-precision numerical integration, we next systematically explore attractors in the reduced state space via Poincaré maps for both all-to-all coupled and star-like coupled networks. For a star-like network, we obtain phase diagrams of attractors as a function of the synaptic time constant. We also find that there exists a sequence of bifurcations when the coupling strengths vary from inhibition to excitation. For instance, in the star-like network, neurons with fast and excitatory synapses exhibit quasi-chaotic behaviors. This novel state is absent in the all-to-all network and is due in part to the unique connectivity of the graph.

A recent experiment [35] on chemical oscillators and the Belousov-Zhabotinsky (BZ) reaction in star networks demonstrates intriguing temporal phase-locking phenomena. The essential BZ reaction can be reduced to a four-dimensional model [36] that mimics periodic surges in chemical concentrations like spikes. Our analysis may clarify understanding of not only neural circuits but also of other pulse-coupled oscillator systems.

The rest of the paper is organized as follows: we introduce the mathematical model in Sec. 2 and Poincaré maps as a dimensional reduction approach in Sec. 3. The aforementioned analytic function for determining the stability of phase-locked states is derived and studied in Sec. 4. Next, in Sec. 5, we thoroughly explore the attractors in an all-to-all network of three and four neurons and a star network of four neurons. Finally, in Sec. 6, we briefly summarize our results and discuss directions for future research.



## 2 Integrate and Fire Model

We begin by introducing the leaky integrate-and-fire neural model.

The dynamics of a network of  $N$  spiking neurons are described by the following equations

$$\begin{aligned} \dot{x}_i &= a_i - x_i + \sum_{j=1}^N K_{ij} s_j(t) \quad i = 1, \dots, N \\ \dot{s}_i &= \alpha(-s_i + b_i), \quad \dot{b}_i = -\alpha b_i \end{aligned} \quad (1)$$

Here,  $x_i \in [0, 1]$  represents the normalized membrane voltage of the  $i$ th individual oscillator;  $s_i$  is the synaptic current of the  $i$ th individual oscillator; and  $b_i$  is introduced as an auxiliary variable. Moreover,  $a_i > 1$ ,  $\alpha > 0$ , and  $K_{ij} \in \mathbb{R}$  are constant parameters. Here, the overdots denote differentiation with respect to time  $t$ . Thus  $\dot{x}_i \equiv dx_i/dt$ . The condition  $a_i > 1$  ensures that firing occurs in the absence of coupling. The parameter  $\alpha$  determines the shape of the pulses emitted when an oscillator fires, and  $K_{ij}$  measures how strongly the  $i$ th oscillator is coupled with the  $j$ th oscillator.  $K_{ij} > 0$  corresponds to excitatory coupling, whereas  $K_{ij} < 0$  corresponds to inhibitory coupling.

Firings occur when one or more of the variables  $x_i$  reaches the threshold  $x_i = 1$ . At this instance,  $x_i$  is reset to 0 and  $b_i$  is augmented by  $\alpha$ . Equivalently, if oscillator  $i$  fires at time  $t_0$ ,  $s_i(t)$  is then augmented by the function  $\phi(t - t_0)$ , where  $\phi(t)$  is an  $\alpha$ -function defined as

$$\phi(t) = \alpha^2 t e^{-\alpha t}. \quad (2)$$

In between firings,  $s_i(t)$  obeys the ODE

$$\ddot{s}_i + 2\alpha \dot{s}_i + \alpha^2 s_i = 0. \quad (3)$$

Therefore,  $s_i(t)$  follows the form  $(A + Bt)e^{-\alpha t}$  and decays to 0 in the absence of firing. However, because  $a_i > 1$ , firings will inevitably occur; otherwise,  $s_i(t)$  would decay to 0, but then the  $i$ th oscillator would reach the threshold in finite time [29].

As mentioned in Sec. 1, we will focus on networks with all-to-all coupling and star network coupling. All-to-all coupled systems are systems in which each oscillator is coupled with every other oscillator. Star network coupled systems, in contrast, consist of a central oscillator to which every other oscillator in the system is coupled with. These two connectivity matrices are depicted schematically in Figs. 1 and 2, in which arrows represent a nonzero coupling strength.

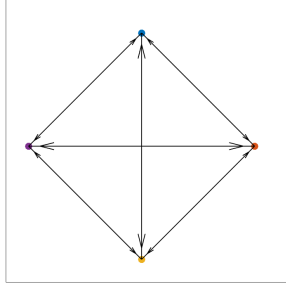


**Figure 1:** Schematic diagram of all-to-all coupled systems.

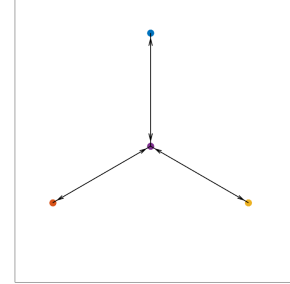


**Figure 2:** Schematic diagram of star network coupled systems.

Finally, note that for a system with  $N$  identical oscillators with uniform all-to-all coupling, we can simplify equation 1 into

$$\begin{aligned} \dot{x}_i &= a_i - x_i + Ks \quad i = 1, \dots, N \\ \dot{s} &= \alpha(-s + b), \quad \dot{b} = -\alpha b \end{aligned} \quad (4)$$

where  $s = \sum_{j=1}^N s_j(t)$  and  $b = \sum_{j=1}^N b_j(t)$ .



Fig. 3 shows the behavior of  $x$  and  $s$  of an LIF neuron. The graphs of  $x$  versus  $t$  illustrate that a neuron exhibits periodic, self-sustained oscillations. The graphs of  $s$  versus  $t$  plotted for two different values of  $\alpha$  illustrate how  $\alpha$  determines the shape of emitted pulses when a neuron fires.

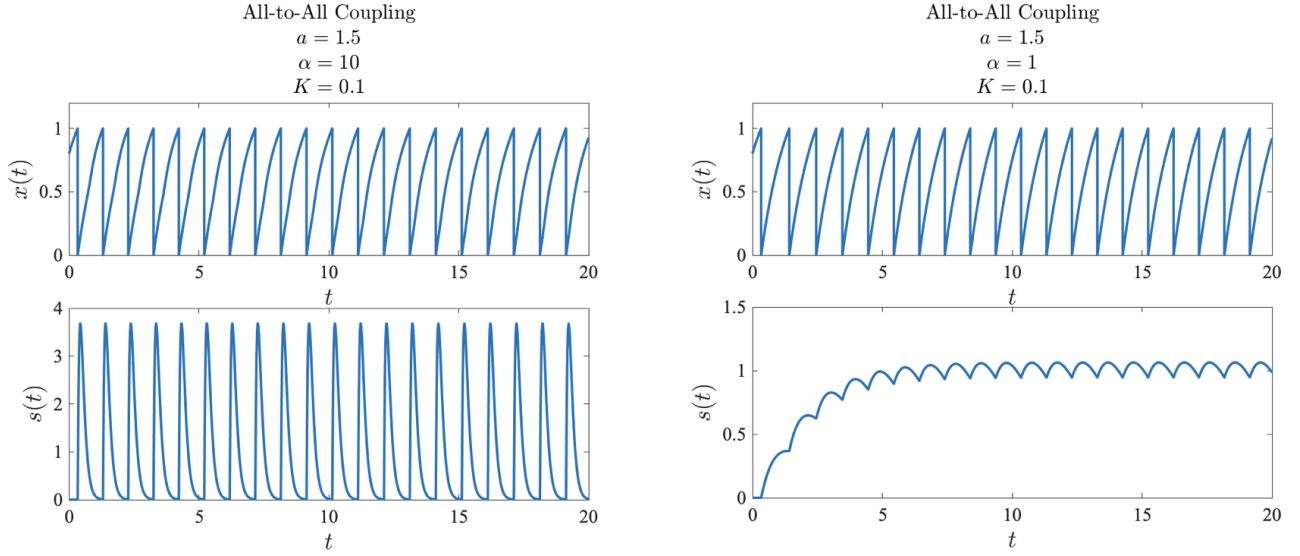


**Figure 3:** Evolutions of  $x$  and  $s$  of an LIF neuron with both fast ( $\alpha = 10$ ) and slow ( $\alpha = 1$ ) synapses.

### 3 Dimensional Reduction

Following Chen *et al.*[29] and Zillmer *et al.*[30], we utilize a Poincaré map to transform the continuously evolving systems described in section 2 into discrete dynamical systems in state spaces of one fewer dimension. Our methodology is as follows: immediately after a selected oscillator fires, we plot the normalized action potentials of the other oscillators in the system. Without the loss of generality, we focus on initial conditions in the fundamental domain  $\mathbf{X}_0$  defined by

$$0 \leq x_{N-1} \leq \dots \leq x_1 < 1 \quad (5)$$

Therefore, an  $N = 3$  system reduces to a flow on the torus  $T^2$ , represented as a unit square. Similarly, an  $N = 4$  system is represented on a unit cube. The boundaries of the fundamental domains consist of cluster synchrony states, in which two or more of the  $x_i$ 's are identical and are invariant under the dynamics [29].

Figs. 4 - 8 show five solution states as Poincaré maps and schematically, if applicable. In each of these figures, we used cell 1 to create a Poincaré section. Figs. 4 - 6 showcase different cluster synchrony states in  $T^3$ , which are steady and time-evolving solutions. Fig. 7 shows the splay state solution in  $T^2$ , where the time difference between two consecutive spikes is constant. Fig. 8 shows the limit cycle solution on  $T^2$ , where the time difference between two consecutive spikes is a fluctuating but periodic pattern. Note that color indicates the flow of time, starting with red, then orange, yellow, green, and so on.

### 4 An Analysis of Phase-Locked Solutions

In this section, we develop an analytic framework to examine phase-locked solutions in all-to-all coupled systems. A phase-locked state is described as follows: each cell fires periodically with same period  $T$  and at a constant phase difference measured relative to the first cell. In other words, if the  $N$ th cell fires at a time  $t_{s,N}$  and the first cell fires at a time  $t_{s,1}$  where  $t_{s,N} < t_{s,1}$ , then the phase difference  $\phi_{s,N} = \frac{t_{s,1} - t_{s,N}}{T}$  is constant. A phase-locked state is shown schematically in Fig. 9.

Given a coupling matrix, we can define a function that captures the phase-locked states as a scalar function. Following the methodology introduced in [34], we extend their work to three cell systems and to the general  $N$ -cell system.

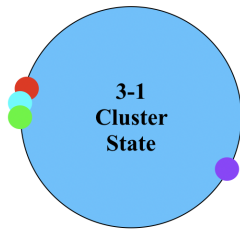
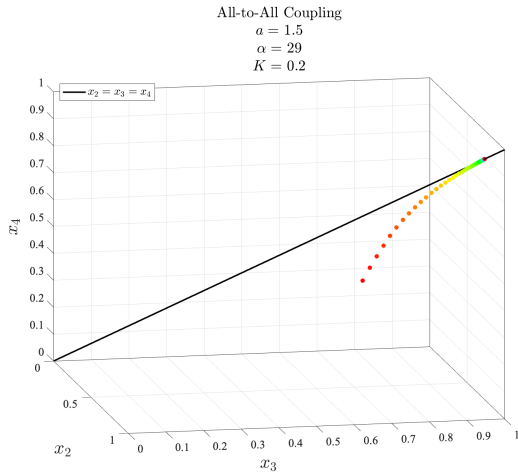


**Figure 4:** 3-1 Cluster synchrony; cells 2-4 synchronized.

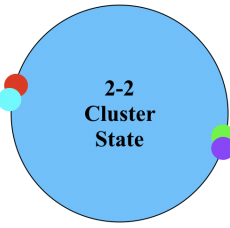
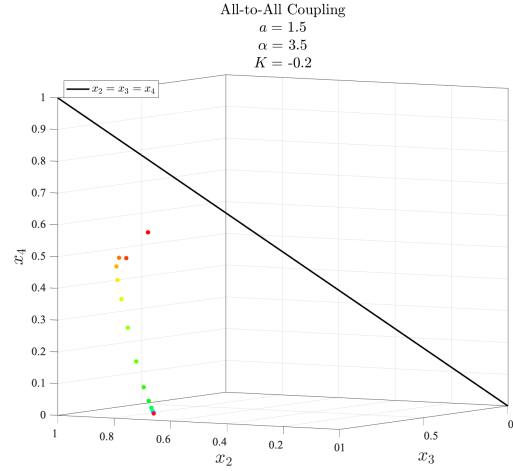


**Figure 5:** 2-2 Cluster synchrony; synchronized clusters of cells 1 and 4, and cells 2 and 3.

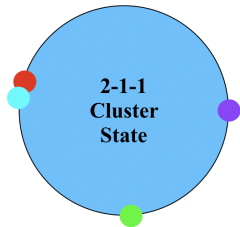
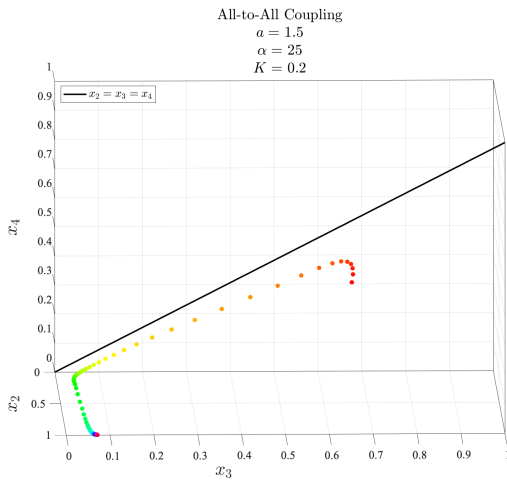


**Figure 6:** 2-1-1 Cluster synchrony, with cells 1 and 4 synchronized. This particular 2-1-1 cluster synchrony happens to be very close to 3-1 cluster synchrony.

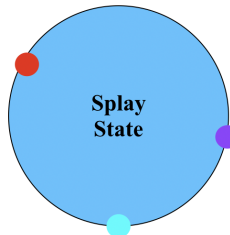
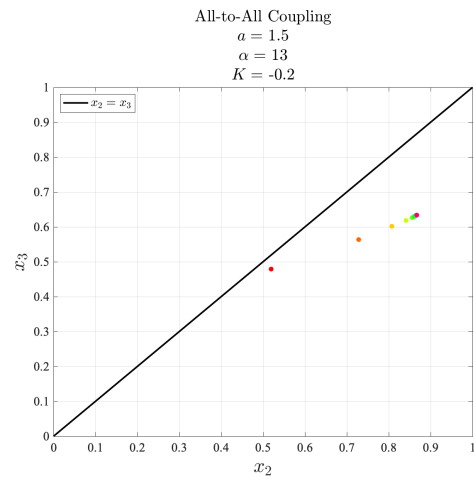


**Figure 7:** Splay state solution, where the time difference between two consecutive spikes is constant.

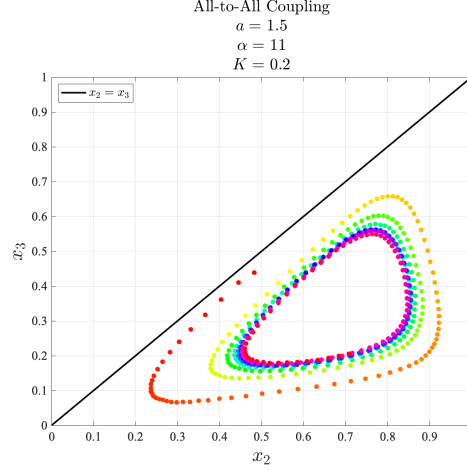


**Figure 8:** Limit cycle solution, a spiraling closed trajectory on the coordinate plane.

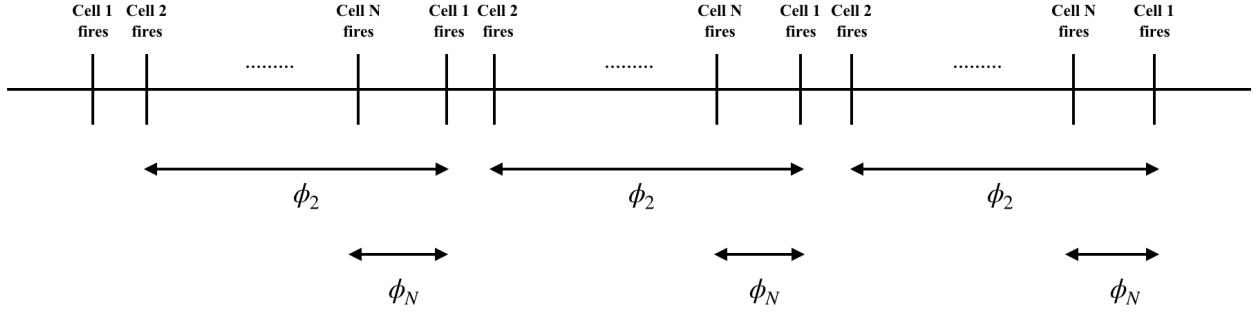


**Figure 9:** Schematic of an  $N$ -cell phase locked state.

#### 4.1 A Review of Two-Cell Systems

We start by reviewing the case of two identical coupled oscillators, studied by van Vreewijsijk *et al.* [34]. We consider cases in which the two cells reach a phase-locked state. Suppose that cell 1 fires periodically at  $t_s = nT = \{\dots, -T, 0, T, \dots\}$  with  $n \in \mathbb{N}$ . Consequently, the synaptic input to cell 2 at  $t = \theta T$  with  $0 < \theta < 1$  is

$$s_{1 \rightarrow 2}(\theta T) = s_T(\theta) \quad (6)$$

where

$$s_T(\theta) = \sum_{n=-\infty}^0 \phi((\theta - n)T) = T\alpha^2 e^{-\alpha\theta T} \frac{\theta(1 - e^{-\alpha T}) + e^{-\alpha T}}{(1 - e^{-\alpha T})^2} \quad (7)$$

Note that our expression for  $s_T$  differs by a factor of  $K$  from [34]. Outside of the range  $0 < \theta < 1$ ,  $s_T(\theta)$  is defined as a periodic function:

$$s_T(\theta - 1) = s_T(\theta) = s_T(\theta + 1). \quad (8)$$

With cell 2 firing at  $t = (n - \phi_2)T$ , the synaptic input to cell 1 is

$$s_{2 \rightarrow 1}(\theta T) = s_T(\theta + \phi_2) \quad (9)$$





Since cell 1 fires at  $t = 0$ , we have  $x_1(0^+) = 0$ . Integrating equation 4 yields

$$x_1(T) = 1 = a(1 - e^{-T}) + KT e^{-T} \int_0^1 e^{\theta T} (s_T(\theta + \phi_2)) d\theta \quad (10)$$

Equation 10 follows from the fact that cell 1 fires again at time  $T$ .

Similarly, cell 2 fires at  $t = -\phi_2 T$  and  $t = (1 - \phi_2)T$ . It follows that

$$x_2((1 - \phi_2)T) = 1 = a(1 - e^{-T}) + KT e^{-T} \int_0^1 e^{\theta T} (s_T(\theta - \phi_2)) d\theta \quad (11)$$

Equations 10 and 11 determine both the period  $T$  and the phase difference  $\phi_2$ . Subtracting (10) from (11) and dividing by  $T$  gives the condition

$$G(\phi_2) = K e^{-T} \int_0^1 e^{\theta T} (s_T(\theta + \phi_2) - s_T(\theta - \phi_2)) d\theta = 0 \quad (12)$$

Clearly,  $\phi_2 = 0$  (and equivalently,  $\phi_2 = 1$ ) is a solution. And because  $s_T(\theta + \frac{1}{2}) = s_T(\theta - \frac{1}{2})$ ,  $\phi_2 = \frac{1}{2}$  is also a solution. These solutions correspond to synchronous and anti-synchronous firing respectively. The sign of  $G'(\phi_2)$  determines stability, where the prime signifies differentiation with respect to  $\phi_2$ .  $G'(\phi_2) > 0$  corresponds to a stable solution;  $G'(\phi_2) < 0$  corresponds to an unstable solution; and  $G'(\phi_2) = 0$  indicates a bifurcation.

The function  $G(\phi_2)$  is plotted in Fig. 10 for three different values of  $\alpha$  in the case of excitatory coupling. When  $\alpha = 4$ , there are three solutions at  $\phi_2 = 0, \frac{1}{2},$  and  $1$ , but only the anti-synchronous solution is stable. At  $\alpha = 5.57$ , a pitchfork bifurcation is born at  $\phi_2 = \frac{1}{2}$  and two additional stable solutions arise. These two additional stable solutions move towards  $\phi_2 = 0$  and  $\phi_2 = 1$  as  $\alpha$  increases, shown for  $\alpha = 6$ . In Fig. 11, we have plotted the inhibitory case; the same set of solutions exist, but the stability is reversed.

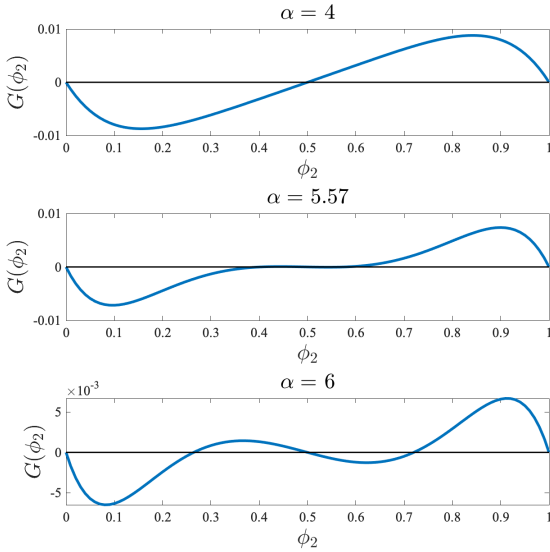


**Figure 10:**  $G$  plotted as a function of  $\phi_2$  for excitatory coupling, with three different values of  $\alpha$  shown.

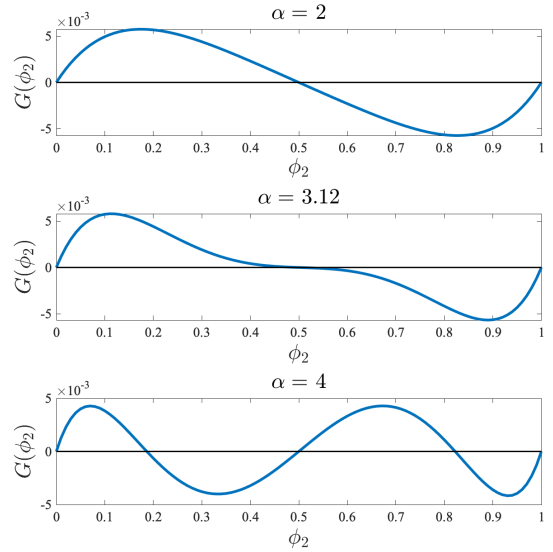


**Figure 11:**  $G$  plotted as a function of  $\phi_2$  for inhibitory coupling, with three different values of  $\alpha$  shown.



## 4.2 Three-Cell Systems

We now extend the work in section 4.1 to a three-cell system. By assuming cell 1 fires periodically at  $t_s = nT = \{\dots, -T, 0, T, \dots\}$ ; cell 2 fires periodically at  $t = (n - \phi_2)T$ ; and that cell 3 fires periodically at  $t = (n - \phi_3)T$  with  $n \in \mathbb{N}$ , we can derive a set of three equations very similar to equations 10 and 11:

$$x_1(T) = 1 = a(1 - e^{-T}) + KTe^{-T} \int_0^1 e^{\theta T} (s_T(\theta + \phi_2) + s_T(\theta + \phi_3)) d\theta \quad (13)$$

$$x_2((1 - \phi_2)T) = 1 = a(1 - e^{-T}) + KTe^{-T} \int_0^1 e^{\theta T} (s_T(\theta - \phi_2) + s_T(\theta - \phi_2 + \phi_3)) d\theta \quad (14)$$

$$x_3((1 - \phi_3)T) = 1 = a(1 - e^{-T}) + KTe^{-T} \int_0^1 e^{\theta T} (s_T(\theta - \phi_3) + s_T(\theta + \phi_2 - \phi_3)) d\theta \quad (15)$$

Similar to that of the two-cell case, these three equations determine both the period  $T$  and the phase differences  $\phi_2$  and  $\phi_3$ . Subtracting (14) from (13) and dividing by  $T$  gives the condition

$$G_1(\phi_2, \phi_3) = Ke^{-T} \int_0^1 e^{\theta T} (s_T(\theta + \phi_2) + s_T(\theta + \phi_3) - s_T(\theta - \phi_2) - s_T(\theta - \phi_2 + \phi_3)) d\theta = 0 \quad (16)$$

Similarly, subtracting (15) from (13) and dividing by  $T$  gives the condition

$$G_2(\phi_2, \phi_3) = Ke^{-T} \int_0^1 e^{\theta T} (s_T(\theta + \phi_2) + s_T(\theta + \phi_3) - s_T(\theta - \phi_3) - s_T(\theta + \phi_2 - \phi_3)) d\theta = 0 \quad (17)$$

We want to find all pairs  $(\phi_2, \phi_3)$  that are zero solutions of  $G_1$  and  $G_2$ , which represent the eventual locations that the trajectories will flow towards. Clearly, the splay state solution  $(\frac{2}{3}, \frac{1}{3})$  is a solution as

$$G_1\left(\frac{2}{3}, \frac{1}{3}\right) = Ke^{-T} \int_0^1 e^{\theta T} (s_T(\theta + \frac{2}{3}) + s_T(\theta + \frac{1}{3}) - s_T(\theta - \frac{2}{3}) - s_T(\theta - \frac{1}{3})) d\theta = 0$$

$$\text{and } G_2\left(\frac{2}{3}, \frac{1}{3}\right) = Ke^{-T} \int_0^1 e^{\theta T} (s_T(\theta + \frac{2}{3}) + s_T(\theta + \frac{1}{3}) - s_T(\theta - \frac{1}{3}) - s_T(\theta + \frac{1}{3})) d\theta = 0$$

since  $s_T$  is periodic. Note that  $(\frac{1}{3}, \frac{2}{3})$  is a splay state solution as well and is also a zero solution to  $G_1$  and  $G_2$ , but we focus on initial conditions in the fundamental domain defined by (5). In Figs. 12 - 15, we have created surfaces of  $G_1$  and  $G_2$  for both inhibitory and excitatory coupling, with the Poincaré map trajectories imposed onto each surface. Just like in section 3, color again represents time. The trajectory starts at red and then flows towards orange, yellow, green, and so on.

We note the trajectories in Figs. 12 - 15 end at coordinates  $(\phi_2, \phi_3)$  where  $G_1 = G_2 = 0$ , as expected. We also note that the trajectories follow the direction of the gradient, which aligns with the conclusions outlined in section 4.1. The trajectories in Figs. 12 - 13 are attracted towards the full synchrony state. In contrast, the trajectories in Figs. 12 - 13 are attracted towards a 2-1 cluster synchrony state.

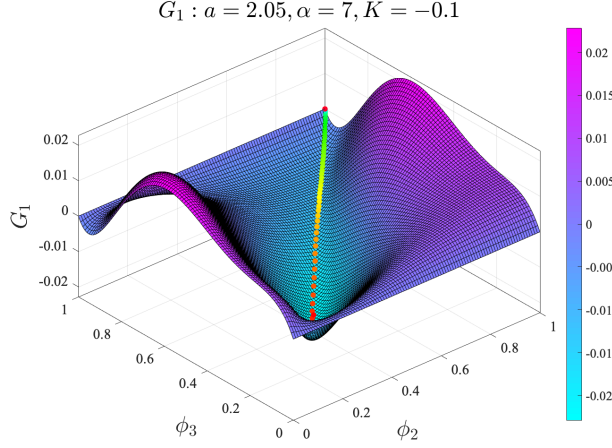


**Figure 12:**  $G_1$  plotted as a function of phase differences  $\phi_2$  and  $\phi_3$  for inhibitory coupling.

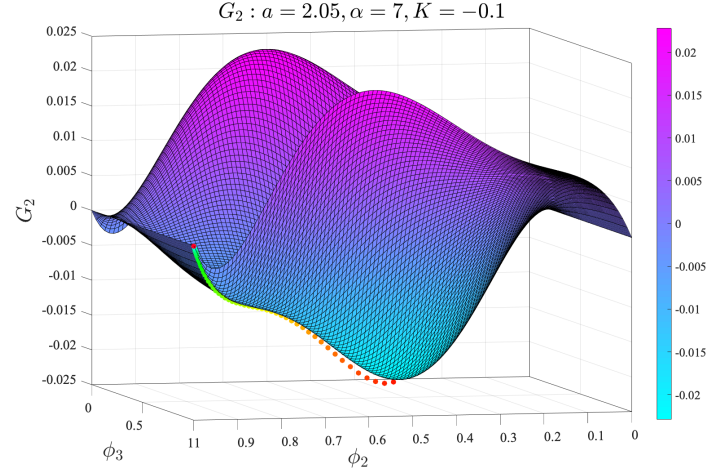


**Figure 13:**  $G_2$  plotted as a function of phase differences  $\phi_2$  and  $\phi_3$  for inhibitory coupling.

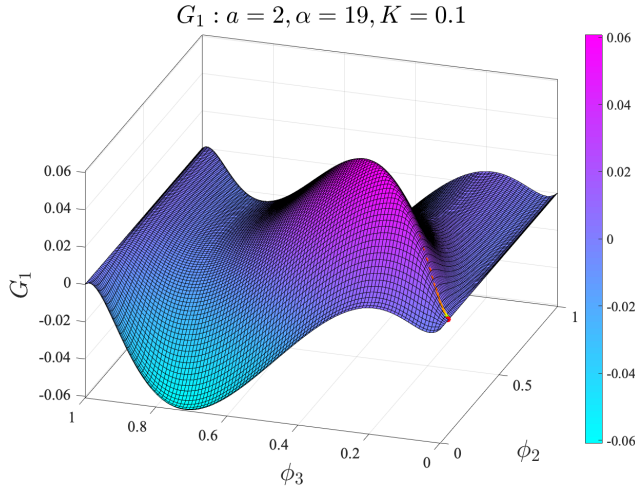


**Figure 14:**  $G_1$  plotted as a function of phase differences  $\phi_2$  and  $\phi_3$  for excitatory coupling.

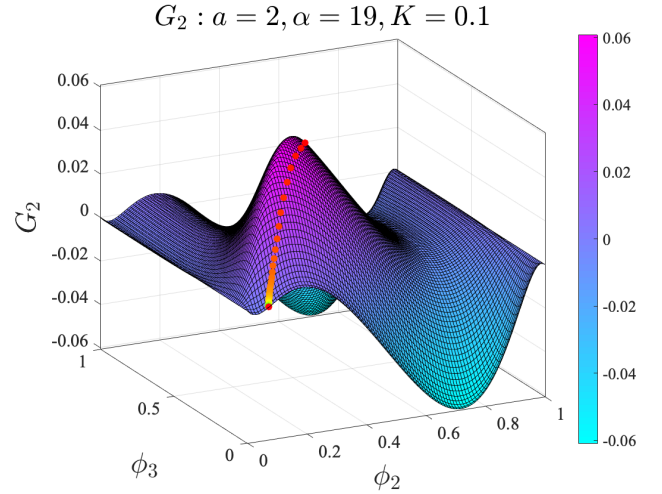


**Figure 15:**  $G_2$  plotted as a function of phase differences  $\phi_2$  and  $\phi_3$  for excitatory coupling.

### 4.3 Higher Order Systems

We can extend the G-function to describe the phase-locked dynamics of higher order systems.

For a general  $N$ -cell neural network, assume that cell  $N$  is separated from cell 1 by a phase difference of  $\phi_N$  as in Fig. 9. Following a similar derivation procedure as that of sections 4.1 and 4.2, we find that there will be  $N - 1$  G-functions. The  $M$ th G-function, where  $1 \leq M < N$ , has the form

$$G_M(\phi_2, \phi_3, \dots, \phi_N) = Ke^{-T} \int_0^1 e^{\theta T} \left( \sum_{k=2}^N s_T(\theta + \phi_k) - s_T(\theta - \phi_{M+1}) - \sum_{n=2}^N s_T(\theta + \phi_k - \phi_{M+1}) \right) d\theta = 0. \quad (18)$$

As in section 4.2, a solution's stability is again determined by the sign of the gradient.



## 5 Dynamics of Small Networks with Different Symmetries and Connectivity

In this section, we describe the dynamics of Poincaré maps as a function of the parameter  $\alpha$ . This section centers on three-cell and four-cell systems with different coupling matrices. Our results are based on precise numerical simulations for fixed finite coupling strength  $K$  and fixed  $a$ .

### 5.1 All-to-All Coupling

#### 5.1.1 Three-Cell System

We start by reviewing the dynamics of three identical all-to-all coupled oscillators, studied in Ref. [29] *et al* with very small coupling strengths  $K \rightarrow 0$ . Although Ref. [29] uses a perturbative method with  $K = \pm 0.01$ , we use numerical simulations to observe the same sequence of attractor states as a function of  $\alpha$ .

We first review inhibitory coupling. For very small  $\alpha$ , the system falls into a 2-1 cluster synchrony. As  $\alpha$  increases, we observe both 2-1 cluster synchrony solutions and full synchrony solutions. Finally, for large  $\alpha$ , we can observe full synchrony, 2-1 cluster synchrony, and the splay state solution.

We next consider excitatory coupling. For small  $\alpha$ , the system can fall into a splay state or a 2-1 cluster synchrony. Upon increasing  $\alpha$ , the splay state solution undergoes a Hopf bifurcation, becoming a limit cycle. And as  $\alpha$  increases further, the system bifurcates again and falls into either a 2-1 cluster synchrony or a full synchrony.

Fig. 16 shows the basin of attraction for these solution states given fixed parameters of  $a$ ,  $\alpha$ , and  $K$ . We obtain these results by integrating the system from a large set of varying initial conditions and determining the eventual solution state. As in Sec. 3, we use initial conditions in which  $x_1 \leq x_2 \leq x_3 \leq 1$ . Each colored square represents a different initial condition. From the top sub-figure that shows inhibitory coupling, we see that the splay state has the largest basin of attraction. And in the bottom sub-figure showing excitatory coupling, the limit cycle solution has the largest basin of attraction.

Fig. 17 shows the size basin of attraction of different solution states represented as normalized area, for different values of  $\alpha$  and for both inhibitory coupling and excitatory coupling. We can estimate the probability of observing a given solution state. For instance, in excitatory coupling, the full synchrony solution has a very small basin of attraction compared to the other solution states.

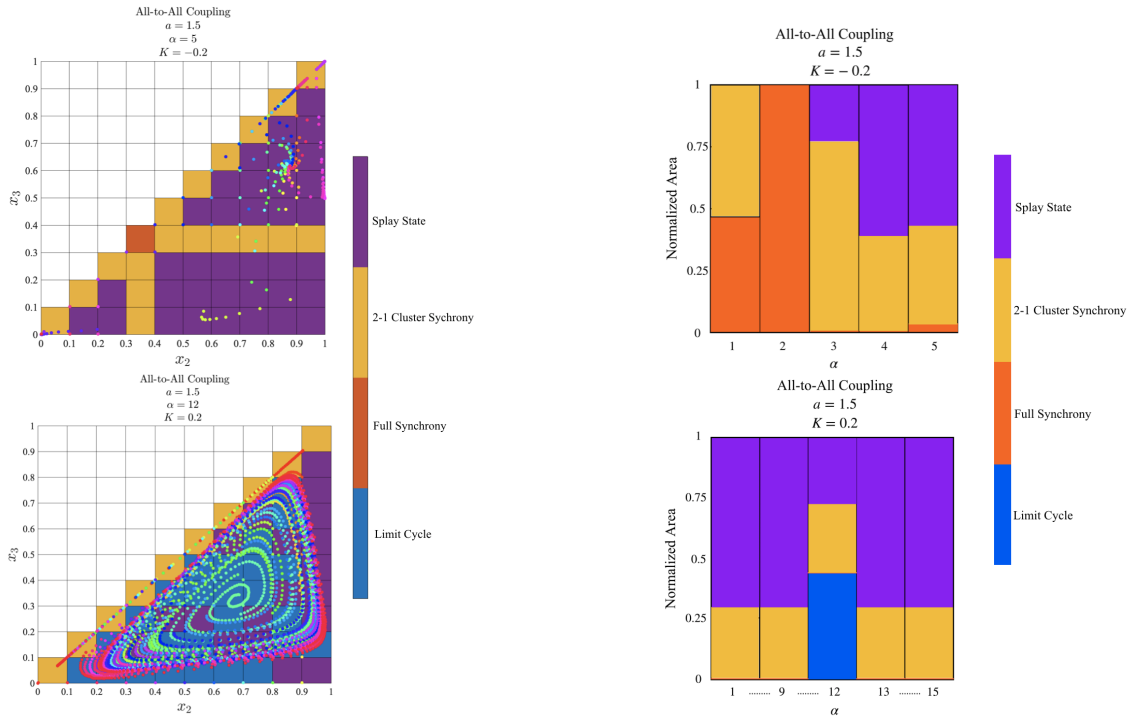


**Figure 16:** Basin of Attraction. Top:  $a = 1.5, \alpha = 5, K = -0.2$ . Bottom:  $a = 1.5, \alpha = 12, K = 0.2$ .

**Figure 17:** Basin of attraction of different solution states represented as a function of  $\alpha$ .



### 5.1.2 Four-Cell System

We now review the dynamics of four identical all-to-all coupled oscillators. The sequence of solutions is very similar to that of the three-cell case, but we observe a richer set of attractors.

We first analyze inhibitory coupling, with  $K = -0.2$ . The sequence of attractor states is shown in Figs. 18 and 19. For small  $\alpha$ , the system is attracted towards full synchrony. As  $\alpha$  increases, a saddle node on the  $x_4 = 0$  face appears, an attracting direction normal to the face and repelling direction along the edge towards full synchrony. As  $\alpha$  further increases, the solution state becomes a 2-2 cluster synchrony, and the saddle node becomes an attractor. Finally, for larger values of  $\alpha$ , the system falls into a stable splay state.

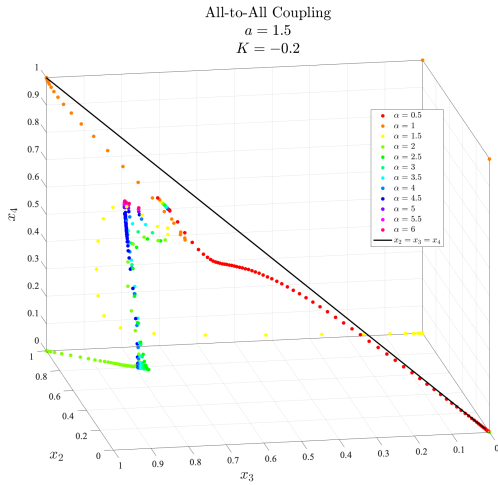


**Figure 18:** The Poincaré maps plotted for  $\alpha = 0.5 - 6$ , displaying the progression from full synchrony to 2-2 cluster states to splay states.

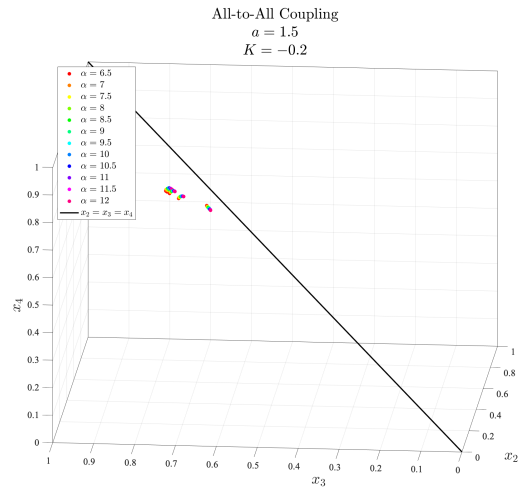


**Figure 19:** The Poincaré maps plotted for  $\alpha = 6.5 - 12$ , displaying the stable splay state solution.

We now consider the excitatory case, simulated with  $K = 0.2$ . See Figs. 20 and 21 for the sequence of attractor states. For small  $\alpha$ , the system falls into a splay state. As  $\alpha$  increases, the splay state bifurcates into a limit cycle. The limit cycle is attracting, and the size of the orbit increases with  $\alpha$ . Up until a critical value of  $\alpha_c$ , the limit cycle solution flows inward. Once  $\alpha$  reaches  $\alpha_c$ , the system bifurcates once again and the limit cycles flows outward. As  $\alpha$  increases further, the limit cycle falls onto the boundary of the cube and breaks down, shown in Fig. 20 at  $\alpha = 24.5$ . After this point, we observe both the 2-1-1 cluster states for smaller values of  $\alpha$  and 3-1 cluster states for larger values of  $\alpha$ .

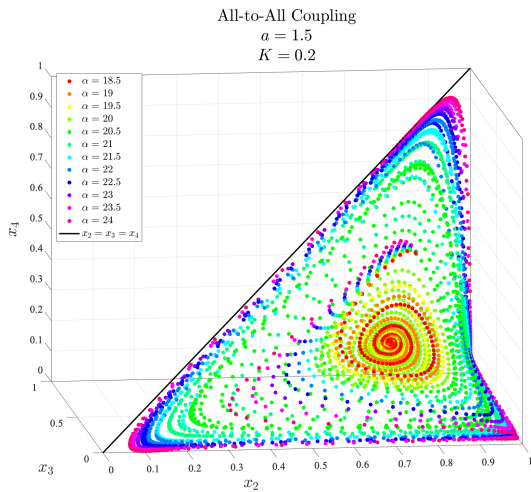


**Figure 20:** The Poincaré maps plotted for  $\alpha = 18.5 - 24$ , showcasing the limit cycle solution.

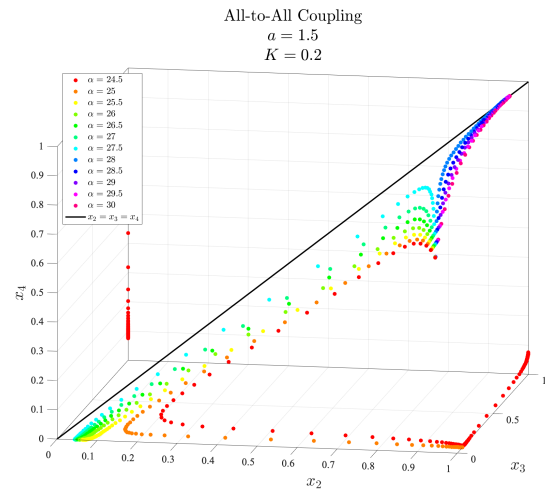


**Figure 21:** The Poincaré maps plotted for  $\alpha = 24.5 - 30$ , displaying the breakdown of the limit cycle solution.



## 5.2 Star Network Coupling

In this section, we discuss the rich dynamics of star network coupled 4-cell system. We first discuss how the unique structure of the coupling matrix can affect the dynamics of the neural network. We then describe the dynamics of inhibitory and excitatory-coupled systems in greater detail, focusing on the rich patterns and symmetries as a function of  $\alpha$ . We will refer to the central oscillator as cell 4, to which cells 1, 2, and 3 are each coupled with.

### 5.2.1 General Discussion

First, with inhibitory coupling, cell 4 is so strongly inhibited that it fires far fewer times than the other cells in the network. In fact, for small enough values of  $\alpha$ , we may observe an oscillation death of cell 4. We therefore use cell 1 to generate the Poincaré maps shown in Fig. 22. In contrast, with excitatory, cell 4 is so strongly excited that it fires many more times than the other cells in the network. We therefore use cell 4 to generate the Poincaré maps in Fig. 23. These dynamics are studied in greater detail in subsection 5.2.2.

Second, as noted in Sec. 1, the symmetry of connectivity can provide a guidance in determining the final solution state. In Figs. 22 and 23 below, we have plotted the Poincaré maps of inhibitory and excitatory systems with three different connectivity matrices.

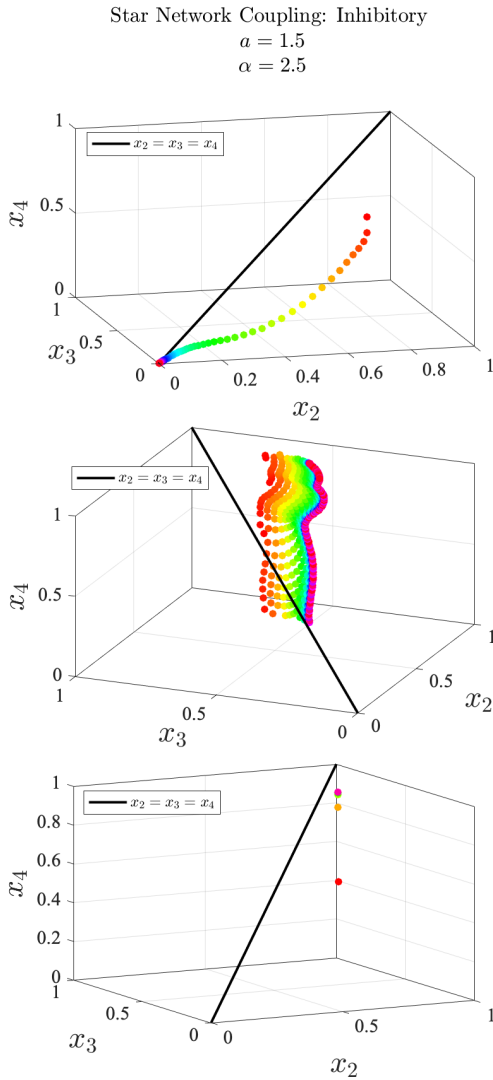


**Figure 22:** Poincaré maps plotted for inhibitory coupling, with three different connectivity matrices.

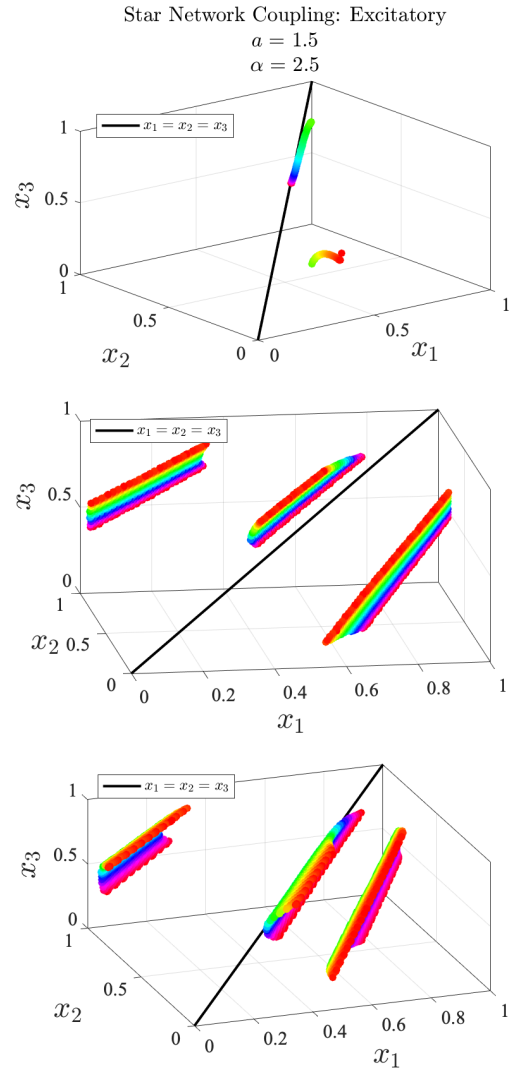


**Figure 23:** Poincaré maps plotted for excitatory coupling, with three different connectivity matrices.



The top sub-figures are generated with a coupling matrix  $A$  of the form

$$A = K \begin{pmatrix} 0 & 0 & 0 & 1 \\ 0 & 0 & 0 & 1 \\ 0 & 0 & 0 & 1 \\ \frac{1}{3} & \frac{1}{3} & \frac{1}{3} & 0 \end{pmatrix} \quad (19)$$

where  $K = -0.2$  in Fig. 22 and  $K = 0.2$  in Fig. 23. The motivation behind using this coupling matrix is to ensure that the collective input from cells 1-3 to cell 4 is the same as the input from cell 4 to each of those three cells. We observe that with this coupling structure, the dynamics behave similar to that of the all-to-all case: full synchrony for inhibitory coupling and a splay state (close to 3-1 cluster synchrony) for excitatory coupling.

The middle sub-figures are generated with a coupling matrix  $A$  of the form

$$A = K \begin{pmatrix} 0 & 0 & 0 & 1 \\ 0 & 0 & 0 & 1 \\ 0 & 0 & 0 & 1 \\ \frac{2}{3} & \frac{2}{3} & \frac{2}{3} & 0 \end{pmatrix} \quad (20)$$

with the aforementioned  $K$  values. With this coupling matrix, the collective input from cells 1-3 to cell 4 is twice the amount of input from cell 4 to each of the other three cells. We observe that this increase in synaptic input causes the system to bifurcate, resulting in the unique trajectories showcased. The inhibited system's rich dynamics is due to cells 1, 2, 3 being in a limit cycle while cell 4 fires slowly. In the excited system, cells 1, 2, 3 are also in a limit cycle while cell 4 fires very rapidly.

The bottom sub-figures are generated with a coupling matrix  $A$  of the form

$$A = K \begin{pmatrix} 0 & 0 & 0 & 1 \\ 0 & 0 & 0 & 1 \\ 0 & 0 & 0 & 1 \\ 1 & 1 & 1 & 0 \end{pmatrix} \quad (21)$$

with the same  $K$  values as before. Here, the collective input from cells 1-3 to cell 4 is three times the amount of input from cell 4 to each of the other cells. This increase in synaptic input causes the inhibited system to bifurcate again, resulting in a new solution state: the death of an oscillator. The excited system exhibits the same behavior as before.

### 5.2.2 Uniform Star Network Coupled Systems

In this section, we comprehensively describe the dynamics of star network coupled four-cell system with uniform coupling; i.e. the coupling matrix is of the form in equation 21.

The phase diagram of attractor states as a function of  $\alpha$  for both inhibitory and excitatory coupling is shown schematically in Fig. 24.

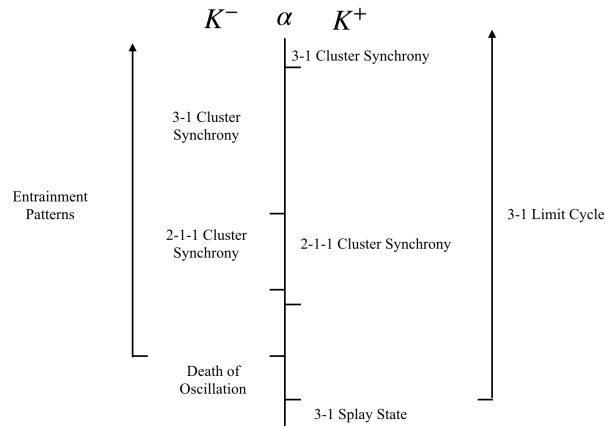


**Figure 24:** Schematic phase diagrams of attractor states as a function of  $\alpha$ .



We first examine inhibitory coupling. For small  $\alpha$ , we observe an oscillation death of the central oscillator. This phenomenon is a result of the strong inhibition. From Fig. 25, we see that cells 1, 2, and 3 inhibit the central oscillator so strongly that it is prevented from firing. Increasing  $\alpha$  revives cell 4 and the systems falls into entrainment patterns. This means that the system displays a firing pattern characteristic of Fig. 26. Cells 1, 2, and 3 will fire in that order several times before cell 4 fires. Upon increasing  $\alpha$  even further, the system bifurcates and cluster synchrony states are born. We observe stable 2-1-1 cluster synchrony states for intermediate range of  $\alpha$  and 3-1 cluster synchrony states for large  $\alpha$ .

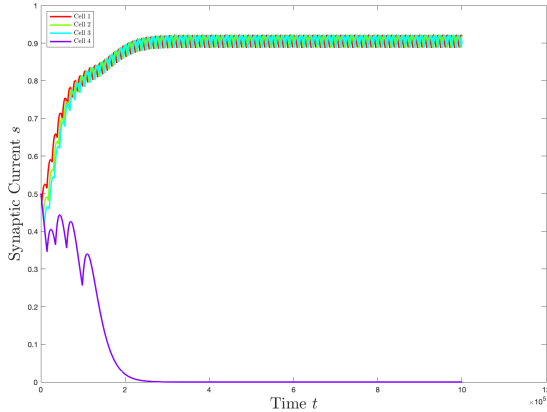


**Figure 25:** Plot of the synaptic currents  $s$ , simulated with  $K = -0.2$ ,  $a = 1.5$ , and  $\alpha = 0.5$ . Shows the death of oscillation of cell 4.

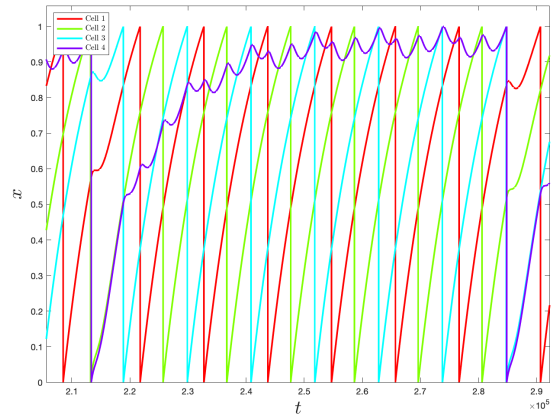


**Figure 26:** Plot of the action potentials  $x$ , simulated with  $K = -0.2$ ,  $a = 1.5$ , and  $\alpha = 12.5$ . Illustrates entrainment patterns.

We next examine excitatory coupling. These dynamics are particularly rich, as the solutions are time-evolving. For small  $\alpha$ , cells 1, 2, and 3 will form a splay state, while cell 4 fires rapidly. We call this phenomenon a "3-1 splay state," shown in Fig. 27. Then, at some critical  $\alpha_c$ , the system bifurcates and cells 1, 2, and 3 form a limit cycle – similar to the all-to-all case. However, this gives rise some many interesting patterns. We may observe behaviors that look like the limit cycle in the all-to-all coupled case, shown in Fig. 28. It is also possible for these three cells to synchronize while remaining in limit cycle, due to uniqueness of the connectivity matrix. For large  $\alpha$ , we observe stable 2-1-1 cluster synchrony states, where the synchronized cluster is any two of the cells 1, 2, and 3. And for very large  $\alpha$ , we observe 3-1 cluster synchrony states, where cells 1, 2, and 3 are synchronized.

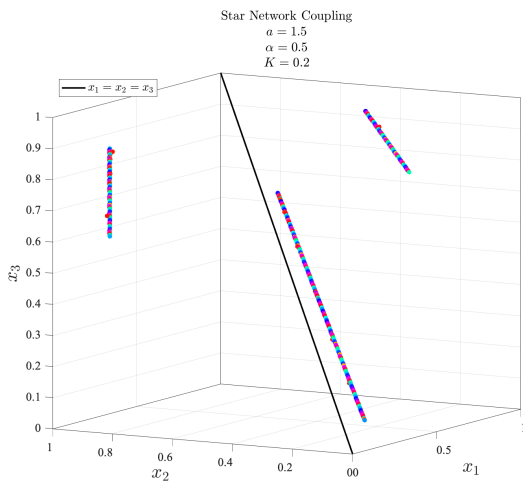


**Figure 27:** 3-1 Splay state solution in a star network. Here, cells 1, 2, and 3 form a splay state while cell 4 fires rapidly, corresponding to straight lines.

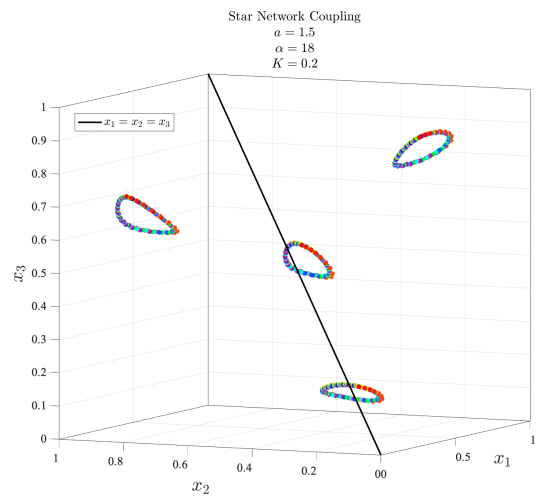


**Figure 28:** 3-1 Limit cycle solution in a star network. Cells 1, 2, and 3 form a limit cycle while cell 4 fires rapidly.





## 6 Discussion

We have systematically studied the dynamics of the reduced state space via Poincaré maps for both all-to-all coupled and star-like networks. In section 4, we developed a set of analytic functions to describe the stability of phase-locked states. The behavior of our derived equations aligns with the results of numerical simulations. And in section 5, we thoroughly explored the rich patterns exhibited in a star network, revealing novel states unobserved in the all-to-all network: the death of oscillation for slow and inhibitory synapses and a quasi-chaotic pattern for fast and excitatory synapses.

One important direction for future research is to extend the G-function introduced in section 4 to star networks. The proof in section 4 assumes a phase-locked system, but the system in a star-like network is not phase-locked but rather time-evolving. One possible approach for inhibitory coupling is to use the entrainment patterns: if we know that cells 1, 2, and 3 collectively fire  $x$  times before cell 4 fires, we may be able to derive equations that capture the behavior of the system.

Another direction for future research is to clarify the role that connectivity plays in system dynamics. As we noted in sections 1 and 5.2.1, the strength of the connection between cell 4 and the other three cells clearly affects system dynamics. After all, as the strength increases, an inhibited system progresses from full synchrony to oscillation death and an excited system progresses from a stable splay state to time-evolving solutions. In the future, we hope to uncover the responsible sequence of bifurcations.

In the continuum limit ( $N \rightarrow \infty$ ), the conventional approach of studying its dynamics is via a mean-field "order parameter" which is a weighted average of all oscillators' configuration. Many efforts focus on the stability of the fully synchronized states and the fully asynchronous splay states. However, many real systems [6, 35] have finite number of cells ( $N \sim 10^1$ ). The mean-field approach breaks down due to strong temporal fluctuations. Indeed, as we have seen in this paper, the overall picture of attractors for small  $N$  is much richer than a competition between sync and splay. Therefore, our results shed lights on connecting symmetries and patterns in dynamical systems with finite degrees of freedom.



## References

- [1] John Buck. Synchronous rhythmic flashing of fireflies. ii. *The Quarterly review of biology*, 63(3):265–289, 1988.
- [2] Charles S. Peskin. Mathematical aspects of heart physiology. 1975.
- [3] AE Dolbear. The cricket as a thermometer. *The American Naturalist*, 31(371):970–971, 1897.
- [4] Andrea Ravignani, Daniel L Bowling, and W Fitch. Chorusing, synchrony, and the evolutionary functions of rhythm. *Frontiers in psychology*, 5:1118, 2014.
- [5] Eve Marder and Ronald L Calabrese. Principles of rhythmic motor pattern generation. *Physiological reviews*, 76(3):687–717, 1996.
- [6] Eve Marder and Dirk Bucher. Central pattern generators and the control of rhythmic movements. *Current biology*, 11(23):R986–R996, 2001.
- [7] Lauren M Jones, Alfredo Fontanini, Brian F Sadacca, Paul Miller, and Donald B Katz. Natural stimuli evoke dynamic sequences of states in sensory cortical ensembles. *Proceedings of the National Academy of Sciences*, 104(47):18772–18777, 2007.
- [8] Margaret F Carr, Shantanu P Jadhav, and Loren M Frank. Hippocampal replay in the awake state: a potential substrate for memory consolidation and retrieval. *Nature neuroscience*, 14(2):147, 2011.
- [9] Paul Miller and Donald B Katz. Stochastic transitions between neural states in taste processing and decision-making. *Journal of Neuroscience*, 30(7):2559–2570, 2010.
- [10] Wolfgang Maass and Henry Markram. On the computational power of circuits of spiking neurons. *Journal of computer and system sciences*, 69(4):593–616, 2004.
- [11] Samanwoy Ghosh-Dastidar and Hojjat Adeli. Spiking neural networks. *International journal of neural systems*, 19(04):295–308, 2009.
- [12] H elene Paugam-Moisy and Sander Bohte. Computing with spiking neuron networks. *Handbook of natural computing*, pages 335–376, 2012.
- [13] David Daniel Cox and Thomas Dean. Neural networks and neuroscience-inspired computer vision. *Current Biology*, 24(18):R921–R929, 2014.
- [14] Adam H Marblestone, Greg Wayne, and Konrad P Kording. Toward an integration of deep learning and neuroscience. *Frontiers in computational neuroscience*, 10:94, 2016.
- [15] Stephen J Verzi, Fredrick Rothganger, Ojas D Parekh, Tu-Thach Quach, Nadine E Miner, Craig M Vineyard, Conrad D James, and James B Aimone. Computing with spikes: The advantage of fine-grained timing. *Neural computation*, 30(10):2660–2690, 2018.
- [16] Terrence J Sejnowski. *The deep learning revolution*. 2018.
- [17] Eugene M Izhikevich. Simple model of spiking neurons. *IEEE Transactions on neural networks*, 14(6):1569–1572, 2003.
- [18] Arkady Pikovsky, Jurgen Kurths, Michael Rosenblum, and J urgen Kurths. *Synchronization: a universal concept in nonlinear sciences*, volume 12. Cambridge university press, 2003.
- [19] Peter Ashwin, Stephen Coombes, and Rachel Nicks. Mathematical frameworks for oscillatory network dynamics in neuroscience. *The Journal of Mathematical Neuroscience*, 6(1):2, 2016.
- [20] James J Collins and Ian N Stewart. Coupled nonlinear oscillators and the symmetries of animal gaits. *Journal of Nonlinear Science*, 3(1):349–392, 1993.
- [21] Martin Golubitsky and Ian Stewart. Patterns of oscillation in coupled cell systems. In *Geometry, mechanics, and dynamics*, pages 243–286. Springer, 2002.
- [22] Martin Golubitsky and Ian Stewart. Nonlinear dynamics of networks: the groupoid formalism. *Bulletin of the american mathematical society*, 43(3):305–364, 2006.
- [23] Martin Golubitsky, Ian Stewart, and David G Schaeffer. *Singularities and groups in bifurcation theory*, volume 2. Springer Science & Business Media, 2012.
- [24] Vincenzo Nicosia, Miguel Valencia, Mario Chavez, Albert D iaz-Guilera, and Vito Latora. Remote synchronization reveals network symmetries and functional modules. *Physical review letters*, 110(17):174102, 2013.
- [25] Louis M Pecora, Francesco Sorrentino, Aaron M Hagerstrom, Thomas E Murphy, and Rajarshi Roy. Cluster synchronization and isolated desynchronization in complex networks with symmetries. *Nature communications*, 5:4079, 2014.



- [26] Francesco Sorrentino, Louis M Pecora, Aaron M Hagerstrom, Thomas E Murphy, and Rajarshi Roy. Complete characterization of the stability of cluster synchronization in complex dynamical networks. *Science advances*, 2(4):e1501737, 2016.
- [27] Renato E Mirollo and Steven H Strogatz. Synchronization of pulse-coupled biological oscillators. *SIAM Journal on Applied Mathematics*, 50(6):1645–1662, 1990.
- [28] LF Abbott and Carl van Vreeswijk. Asynchronous states in networks of pulse-coupled oscillators. *Physical Review E*, 48(2):1483, 1993.
- [29] Bolun Chen, Jan R. Engelbrecht, and Renato Mirollo. Cluster synchronization in networks of identical oscillators with  $\alpha$ -function pulse coupling. *Phys. Rev. E*, 95:022207, Feb 2017.
- [30] Rüdiger Zillmer, Roberto Livi, Antonio Politi, and Alessandro Torcini. Stability of the splay state in pulse-coupled networks. *Phys. Rev. E*, 76:046102, Oct 2007.
- [31] Can Xu, Jian Gao, Stefano Boccaletti, Zhigang Zheng, and Shuguang Guan. Synchronization in starlike networks of phase oscillators. *Physical Review E*, 100(1):012212, 2019.
- [32] Lawrence G Roberts and Barry D Wessler. Computer network development to achieve resource sharing. In *Proceedings of the May 5-7, 1970, spring joint computer conference*, pages 543–549. ACM, 1970.
- [33] Yu Hu, Steven L Brunton, Nicholas Cain, Stefan Mihalas, J Nathan Kutz, and Eric Shea-Brown. Feedback through graph motifs relates structure and function in complex networks. *Physical Review E*, 98(6):062312, 2018.
- [34] Carl Van Vreeswijk, L. F. Abbott, and G. Bard Ermentrout. When inhibition not excitation synchronizes neural firing. *Journal of Computational Neuroscience*, 1(4):313–321, Dec 1994.
- [35] Michael M Norton, Nathan Tompkins, Baptiste Blanc, Matthew C Cambria, Jesse Held, and Seth Fraden. Dynamics of reaction-diffusion oscillators in star networks. *arXiv preprint arXiv:1907.03924*, 2019.
- [36] Vladimir K Vanag and Irving R Epstein. Pattern formation in a tunable medium: The belousov-zhabotinsky reaction in an aerosol of microemulsion. *Physical review letters*, 87(22):228301, 2001.



国际竞赛 科研科创 发表论文  
关注“有方背景提升”

## 7 Acknowledgements

I would like to sincerely thank my mentor Dr. Bolun Chen of Brandeis University for suggesting this project and providing thorough guidance and invaluable advice. I would also like thank Prof. Pavel Etingof, Dr. Slava Gerovitch, and Dr. Tanya Khovanova of the MIT PRIMES Program for providing me with this research opportunity and external guidance. And last but certainly not least, I would like to thank the organizers of the Yau Awards for allowing to share my work.



国际竞赛 科研科创 发表论文  
关注“有方背景提升”

本参赛团队声明所提交的论文是在指导老师指导下进行的研究工作和取得的研究成果。尽本团队所知，除了文中特别加以标注和致谢中所罗列的内容以外，论文中不包含其他人已经发表或撰写过的研究成果。若有不实之处，本人愿意承担一切相关责任。

参赛队员： Victoria Zhang

指导老师： Bolun Chen

2019 年 9 月 7 日